Multifactorial analysis of ion concentration polarization for microfluidic preconcentrating applications using response surface method

Cite as: Phys. Fluids **32**, 072012 (2020); https://doi.org/10.1063/5.0010698 Submitted: 13 April 2020 . Accepted: 09 July 2020 . Published Online: 31 July 2020

Majid Gholinejad 🗓, Ali Jabari Moghadam 🗓, Seyed Ali Mousavi Shaegh 🗓, and Amir K. Miri







ARTICLES YOU MAY BE INTERESTED IN

Effects of gravity and surface tension on steady microbubble propagation in asymmetric bifurcating airways

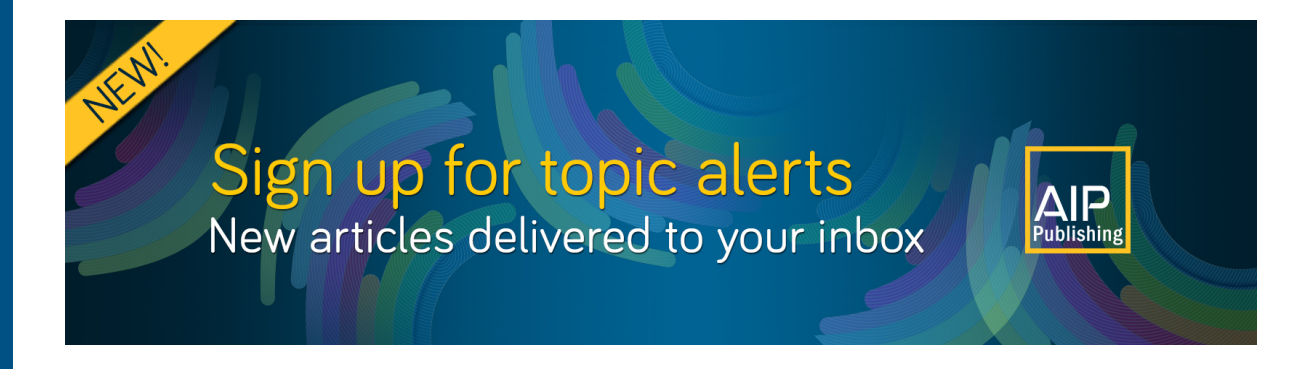
Physics of Fluids 32, 072105 (2020); https://doi.org/10.1063/5.0012796

The translational and rotational motions of a cylindrical particle in a granular shear flow inside a split bottom Couette cell

Physics of Fluids 32, 073310 (2020); https://doi.org/10.1063/5.0015175

Scaling relations in shear electroconvective vortices

Physics of Fluids 32, 072009 (2020); https://doi.org/10.1063/5.0015117





Multifactorial analysis of ion concentration polarization for microfluidic preconcentrating applications using response surface method

Cite as: Phys. Fluids 32, 072012 (2020); doi: 10.1063/5.0010698

Submitted: 13 April 2020 • Accepted: 9 July 2020 •

Published Online: 31 July 2020











Majid Gholinejad, 1,2,3,4 Ali Jabari Moghadam, 1,a) Seyed Ali Mousavi Shaegh, 2,3,4,a) and Amir K. Miri^{5,6}



AFFILIATIONS

- ¹ Faculty of Mechanical Engineering, Shahrood University of Technology, P.O. Box 361, Shahrood, Iran
- Orthopedic Research Center, Mashhad University of Medical Sciences, Mashhad, Iran

Clinical Research Unit, Ghaem Hospital, Mashhad University of Medical Sciences, P.O. Box 91735451, Mashhad, Iran

- ⁴Microfluidics and Medical Microsystems Laboratory, BuAli Research Institute, Mashhad University of Medical Sciences, P.O. Box 9196773117, Mashhad, Iran
- ⁵Biofabrication Lab, Department of Mechanical Engineering, Rowan University, Glassboro, New Jersey 08028, USA
- School of Medical Engineering, Science, and Health, Rowan University, Camden, New Jersey 08103, USA

ABSTRACT

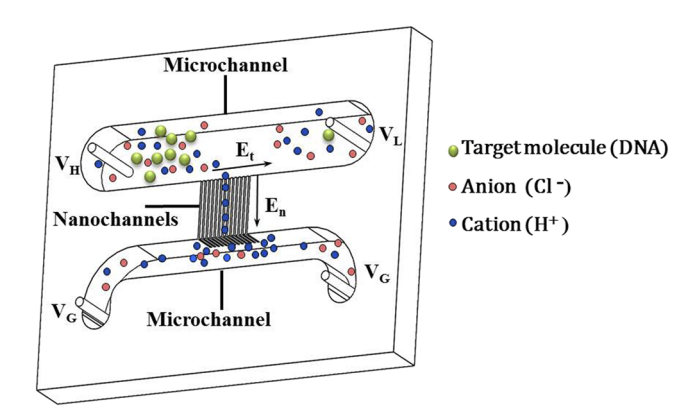
Ion concentration polarization (ICP) in a microfluidic device requires a precise balance of forces on charged molecules to achieve high concentrating efficiency. It is, thus, of considerable interest to study the impact of all governing parameters on ICP performance. Experimental study of the ICP multifactorial phenomenon seems impractical and costly. We report a systematic approach to understand the impacts of governing parameters on the ICP phenomenon using a robust numerical model established in COMSOL Multiphysics®. We varied the buffer concentration, applied voltage, and microchannel length to study their impacts on the ICP phenomenon. Then, we developed a statistical model via the response surface method (RSM) for the numerical results to study the direct and interactive effects of the mentioned parameters on ICP optimization. It was found that the buffer concentration (C_{buffer}) plays a key role in the enrichment factor (EF); however, simultaneous impacts of the applied voltage and channel length must be considered as well to enhance EF. For low buffer concentrations, C_{buffer} < 0.1 mM, the ionic conductivity was found to be independent of C_{buffer} , while for high buffer concentrations, $C_{buffer} > 1$ mM, the ionic conductivity was directly linked to C_{buffer}. In addition, the RSM-based model prediction for a certain buffer concentration (~1 mM) highlighted that an electric field of 20 V/cm-30 V/cm is suitable for the initial design of experiments in ICP microdevices.

Published under license by AIP Publishing. https://doi.org/10.1063/5.0010698

I. INTRODUCTION

Ion concentration polarization (ICP) has been applied in micro- and nanofluidic devices to concentrate charged analytes in microchannels, a simple, functional approach for diagnostics, biosensing, desalination, and power generation. 1,2 When a charged surface in a microchannel is exposed to an electrolyte solution, counterions of the electrolyte are absorbed onto the charged surface, forming an electrical double layer (EDL).3 The charged ions in a microchannel can move under the influence of a tangential electric field (E_t) and cause the motion of the bulk solution (i.e., electroosmotic flow). When nanochannels are created between microchannels, ionic transport is dominated by the surface charge, which results in the creation of ion selectivity, allowing the passage of counterions with overlapping EDL. In this way, ion selectivity of nanochannels induces a strong normal electric field (En) and this affects the ion concentration gradient at the interface of nanoand microchannels (Fig. 1). The presence of nanochannels with charged surfaces in a microchannel leads to ICP under an electric field. The ICP device results in enrichment and depletion zones in

^{a)} Authors to whom correspondence should be addressed: Alijabari@shahroodut.ac.ir and Mousavisha@mums.ac.ir



 $\label{eq:FIG.1} \textbf{FIG. 1}. \ Schematics of ICP-based device. \ V_H: high voltage, V_G: ground voltage, V_L: low voltage, E_t: tangential electric field, and E_n: normal electric field.$

adjacent microchannels. The nanochannels could be created through either nanofabrication methods or implementation of a nanoporous membrane in a microchannel.

ÎCP devices have been mainly developed for desalination, his micro-mixing, for ionic diodes, for and biomedical applications. Several microfluid-based methods have been used for preconcentrating charged analytes, such as DNA or protein including isoelectric focusing, for disease diagnosis. The conventional methods for preconcentrating molecules require large sample volume and have high costs. Hence, many microfluidic devices have been developed to preconcentrate DNA and proteins at low concentrations. Among them, the ICP method is receiving interest due to its simple design and high enrichment factor (EF) (over 10⁴-fold). Hence, microfluidic devices have been developed to preconcentrate DNA and proteins at low concentrations.

To concentrate charged molecules at a certain position in a microchannel, a balance of electroosmotic, electrophoretic, and ion depletion repulsion forces should be achieved.²¹ Thus, governing parameters such as buffer concentration, applied voltage, and geometry design should be controlled. The preconcentration efficiency of a device can be described using the enrichment factor (EF), i.e., the ratio of the final and initial concentrations for the enriched analyte.

Gao et al. ²² demonstrated that for a buffer concentration (Tris-HCl) within the range of 10 mM–60 mM, the fluorescence intensity of fluorescein sodium increased for the buffer concentrations of up to 50 mM. For higher buffer concentrations, the fluorescence intensity reached a plateau and remained constant. Thus, there should be an optimum buffer concentration value that maximizes the EF. Yuan et al. ²³ investigated the effect of bulk solution and voltage on the preconcentration rate and found that the optimal value of KCl concentration (for 10⁻⁶M fluorescein tracer) was close to 10 mM. They stated that for a certain microchannel length, the preconcentration plug disappears as the voltage exceeds 200 V. The result revealed that the deployment of a proper voltage difference through the microchannel is essential to observe analyte preconcentration with a sufficient enrichment factor.

In addition to experimental studies, many numerical studies have been carried out to characterize the ion concentration

polarization phenomenon for various applications. ^{24,25} Wang *et al.* ²⁶ found that the increase in voltage, which enhances electrophoresis force, improves the enrichment factor. However, a balance between the electrophoretic forces and repulsive forces, induced by charged nanochannels, should be achieved to maximize the enrichment factor. In addition to the balance of the mentioned forces on charged analytes, Ouyang *et al.* ²⁷ found that the anion concentration in the buffer solution restricts the increase in the enrichment factor to maintain electroneutrality. Jia and Kim^{28,29} studied the effects of voltage and buffer concentration on particle accumulation in single and V-shaped microchannels. A decrease in the buffer concentration and an increase in voltage enhance the enrichment factor.

Ionic conductivity, which characterizes the performance of an ICP-based device, is mainly determined by the ionic concentration of the buffer solution and the concentration of charged analytes. The ionic conductivity affects the overall motion of charged ions via diffusion, convection, and electro-migration, under an electric field. Hence, the conductivity could be influenced by the channel characteristics (surface charge and dimensions), applied voltage, and bulk solution behavior. Kim et al.³⁰ measured the ionic conductivity of a microchannel with and without a Nafion® nanoporous membrane, concluding that ionic conductivity increased with the increment of buffer concentration. However, the ionic conductivity of the microchannel with an incorporated Nafion membrane is stable after a threshold of buffer concentration ($C_{buffer} \ge 10 \text{ mM}$). Also, Kamcev et al. 31 studied the effect of salt concentration on an ion exchange membrane for desalination application and found that at high salt concentrations (>0.3M), ionic conductivity enhanced with an increase in the salt concentration. The polyelectrolyte-modified nanopore ionic conductivity was found to be larger at a low buffer concentration ($C_{buffer} = 1 \text{ mM}$) and high voltage ($\nabla V = 1000 \text{ mV}$) than for a case with a medium concentration ($C_{buffer} = 50 \text{ mM}$) and low voltage ($\nabla V = 200 \text{ mV}$).³² The ionic conductivity increased with voltage increment when the buffer concentration is medium (10 mM $< C_{buffer} <$ 100 mM). These results revealed that the interaction between the voltage and buffer concentration played a critical role in the overall conductance of micro-/nano-systems, regardless of their geometrical features.

A number of studies have been devoted to analyze the accumulation of charged molecules. In addition, such studies only investigated the individual effects of parameters such as voltage and buffer concentration, and their combined effects on the device performance were not considered. Better understanding of the ICP phenomenon in a microdevice necessitates studying the interactions of all governing parameters. This study was mainly devoted to perform a multifactorial analysis to investigate the effects of buffer concentration, voltage, and microchannel length and their interactions on the enrichment factor and ionic conductivity in an ICP microsystem. The response surface method (RSM) was employed to study the interactions of the governing parameters.

The precision of RSM model predictions was examined through the analysis of variance (ANOVA). The ANOVA was able to determine the significance of each parameter and its contribution to the enrichment factor and ionic conductivity. The results showed that the buffer concentration had a significant impact on the enrichment factor, while the role of geometry and voltage was important for ionic conductivity. The RSM model could provide a practical

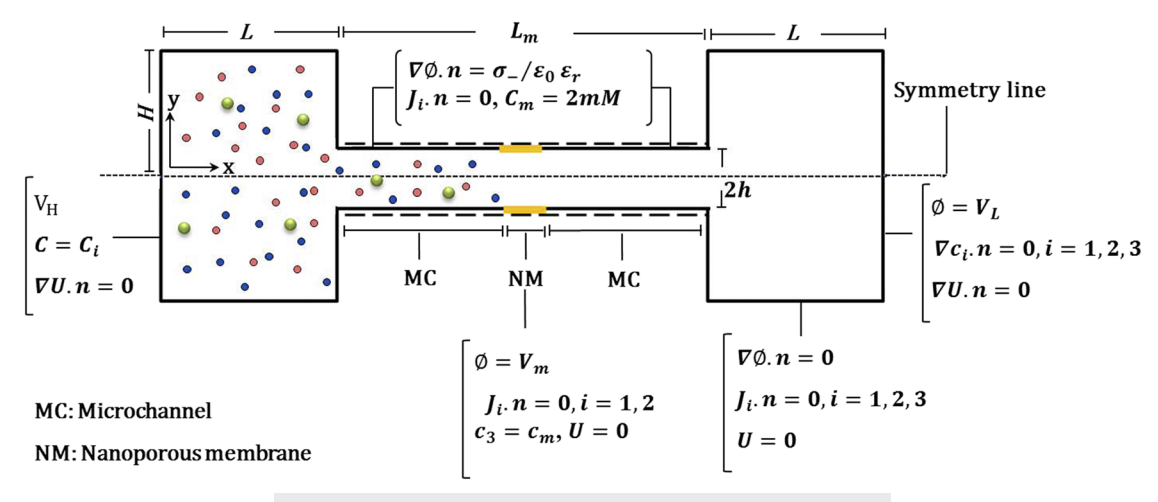


FIG. 2. Geometrical model and boundary conditions for numerical simulation.

approach to design and optimize the performance of ICP-based microdevices for preconcentrating molecules.

II. COMPUTATIONAL DOMAIN AND BOUNDARY CONDITIONS

Figure 2 shows a typical geometry of the ICP-based device studied here. The two side chambers have the dimensions of $50 \times 50 \ \mu \text{m}^2$. The microchannel is located in the midsection of the geometry between the two chambers with a height of $4 \ \mu \text{m}$ ($2h = 4 \ \mu \text{m}$), and its non-dimensional length varies between 30 and 90 (L_m/h : 30–90). The walls of the microchannel had a negative surface charge density of $5 \ \text{mC/m}^2$, and a negatively charged ion-selective membrane was considered to be embedded in the middle of the microchannel ($L_m/2$) with a length of $2 \ \mu \text{m}$ ($L_n = 2 \ \mu \text{m}$). HCl is the buffer solution, and negatively charged DNA molecules are considered as the target molecule (see Table I for the parameters). Over the surface of the membrane, fluxes of negative ions (Cl⁻) and negative DNA

molecules were considered to be zero. The charge of the membrane was assumed to be -2 mM; thus, the concentration of positive ions (H⁺) was considered to be 2 mM. ^{33,34} The dimensionless buffer concentration of HCl varied from 0.01 to 10 (C_{buffer}/C_0 : 0.01–10), and a voltage difference ($\Delta V = V_H - V_L$) was applied to the system in which voltage on the left border (V_H) was higher than that on the right chamber (V_L) . Thus, a tangential electric field was generated and the electroosmotic force could drive the bulk solution through the microchannel. The dimensionless voltage $(\Delta V/V_T)$ ranged from 5 to 30 (thermal voltage V_T = 25.8 mV). In addition, voltage on the membrane's surface (V_m) was set to generate cross-membrane voltage $[V_{cm} = (V_H + V_L)/2 - V_m]$. Normal electric field was then generated, and only cations (H⁺) could pass through the membrane. The cross-membrane voltage (V_{cm}) could affect the enrichment factor until it reached its maximum value. To compare the results in fixed operating conditions and to ensure that the maximum enrichment factor was achieved, the value of $V_{cm}/V_T = 40$ was set for the simulations (Fig. 3).

 TABLE I. Values of constant parameters used in this study.

24,28,29,35,36

Expression	Parameter	Value	Unit
Diffusion coefficient of H ⁺	$D_{ m H^+}$	9.36×10^{-9}	$m^2 s^{-1}$
Diffusion coefficient of Cl	$D_{ m Cl^-}$	2.03×10^{-9}	${ m m}^2 { m s}^{-1}$
Diffusion coefficient of DNA molecule	D_{DNA}	1.51×10^{-10}	${ m m}^2{ m s}^{-1}$
Thermal voltage	V_T	0.0258	V
Microchannel surface charge	σ	-0.005	${ m Cm^{-2}}$
Reference concentration	C_0	1	mM
DNA concentration	$C_{3,0}$	10^{-4}	mM
Viscosity	μ	0.001	Pa s
Microchannel width	2h	4	$\mu\mathrm{m}$
Density	ρ	1000	${\rm kg}{\rm m}^{-3}$

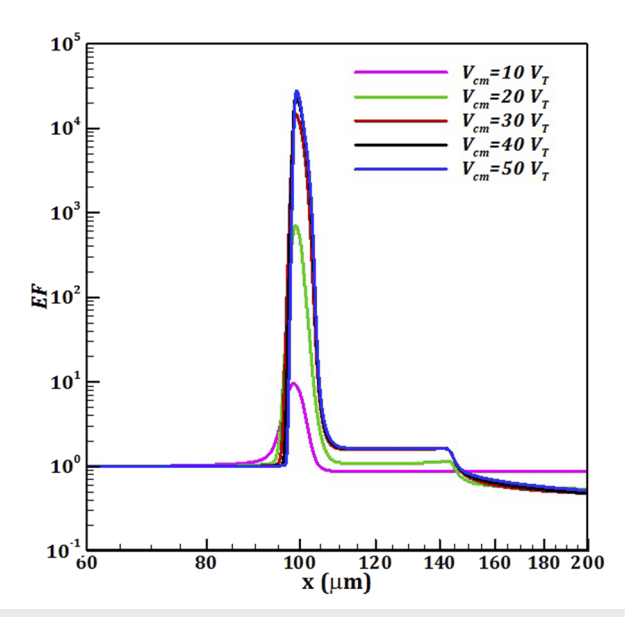


FIG. 3. Variation of the enrichment factor through the microchannel for different cross-membrane voltages at the channel centerline for $L_{m}/h = 84.32$, $\Delta V/V_T = 10.07$, $C_{buffer}/C_0 = 2.03$ derived from COMSOL® simulation.

III. GOVERNING EQUATIONS

The Navier–Stokes equations were solved in the computational domain to obtain the flow-field variables, ^{23,24}

$$\rho(\mathbf{U}\cdot\nabla)\mathbf{U} = -\nabla p + \mu\nabla^2\mathbf{U} - \rho_E\nabla\mathcal{O},\tag{1}$$

where μ is the dynamic viscosity. The last term of Eq. (1) $\rho_E \nabla \emptyset$ is due to the external electric potential of the system that represents the density of net charge inside the solution. To calculate the net charge density, the following equation is used:³³

$$\rho_E = F \sum_i Z_i C_i. \tag{2}$$

Distribution of concentration for different species of ions and DNA molecules in electrolyte solution is obtained by solving the Nernst–Planck equation,³⁵

$$\nabla \cdot \boldsymbol{J_i} = 0, \ \boldsymbol{J_i} = -(D_i \nabla C_i + z_i (D_i F/RT) C_i \nabla \emptyset) + \vec{U} C_i, \tag{3}$$

where C_i , D_i , z_i , and J_i are the concentration, diffusion coefficient, ionic valence, and fluxes of ion species i, respectively. Transport of positive buffer ions (H⁺) is obtained by i = 1, transport of negative buffer ions is obtained by i = 2 (Cl⁻), and the motion of negatively charged molecules (DNA molecules) is obtained by i = 3. The parameter T represents temperature in the standard state (298 K), and F and R represent the Faraday number and the ideal gas constant, respectively.

The Poisson equation was applied to relate ionic concentration to the electric potential, which is expressed as follows: 27

$$\nabla \mathcal{O} = -\rho_E/\varepsilon_0 \varepsilon_r. \tag{4}$$

The above coupled equations were numerically solved.

To evaluate the results, the enrichment factor and ionic conductivity (G) have been used. The enrichment factor is defined as the ratio of the final DNA molecule concentration to its initial concentration ($C_3/C_{3,0}$). For calculating conductivity, the section with the highest value of ionic conductivity was determined for each case and then the integral of conductivity along the width of the microchannel was calculated in that section, ³²

$$G = I/\nabla V = \int_{s} F\left(\sum_{i=1}^{3} z_{i} \mathbf{J}_{i}\right) \cdot n ds / \nabla V.$$
 (5)

IV. GRID INDEPENDENCE STUDY AND VALIDATIONS

Figure 4 shows the solution domain and grid distribution used for the numerical simulation. Due to the geometrical symmetry, the lower half of the system was analyzed to reduce computational cost. Distribution of the grid was selected to be finer in the vicinity of the surfaces for considering the boundary layer around the microchannel walls with charged surface. The extreme changes in target molecule accumulation occur around the membrane's surface. By examining grid sizes of 20 \times 200, 30 \times 300, 40 \times 400, and 50 \times 500 for microchannel length, it was found that for higher grid sizes of 40 \times 400, the enrichment factor and ionic conductivity values converged. The grid size of 40 \times 400 was considered for our computational simulations.

Since there is no 3D simulation in the literature that could be employed for validation purposes, the results of the model were compared with those of Gong *et al.*, ³³ Li *et al.*, ³⁵ and Ouyang *et al.* ²⁷ Figures 5(a) and 5(b) reveal that there is good agreement between the present study and the previously reported ones in terms of distribution of electric potential and sample concentration distribution. In addition, in Fig. S1, the contour of DNA concentration distribution in our model was compared with the experimental and numerical studies of Ouyang *et al.* ²⁷

V. RESPONSE SURFACE METHOD (RSM)

Response surface method (RSM) is an effective method to study several parameters simultaneously and with least possible test designs. We used RSM to study the effects of the buffer concentration, voltage, and microchannel length on the enrichment factor and conductivity. The ranges of the parameters with their levels [low (-1), mean (0), and high (+1) levels] are defined in Table II. Each of the parameters could affect the response (dependent variable), and RSM was a powerful tool to find an appropriate correlation between them. This model could be written as follows:

$$Y = \beta_0 + \sum_{i=1}^{3} \beta_i \chi_i + \sum_{i=1}^{3} \beta_{ii} \chi_i \chi_i + \sum_{i=1}^{3} \beta_{ij} \chi_i \chi_j,$$
 (6)

where Y is the dependent variable [enrichment factor and conductivity (G) in this study], β_0 is the intercept, β_i is the linear regression coefficient of ith factor, β_{ii} is the quadratic regression coefficient of ith factor, and β_{ij} is the interaction of the ith and jth parameters.

To find proper values of β_0 , β_i , β_{ii} , and β_{ij} for solving Eq. (6), a central composite design (CCD) with 20 runs was utilized to cover the range of the parameters. The statistical analysis was carried out by the design of experiment software to relate the effects of the parameters on variables using quadratic model. Table III illustrates the parameters with obtained results from the simulations.

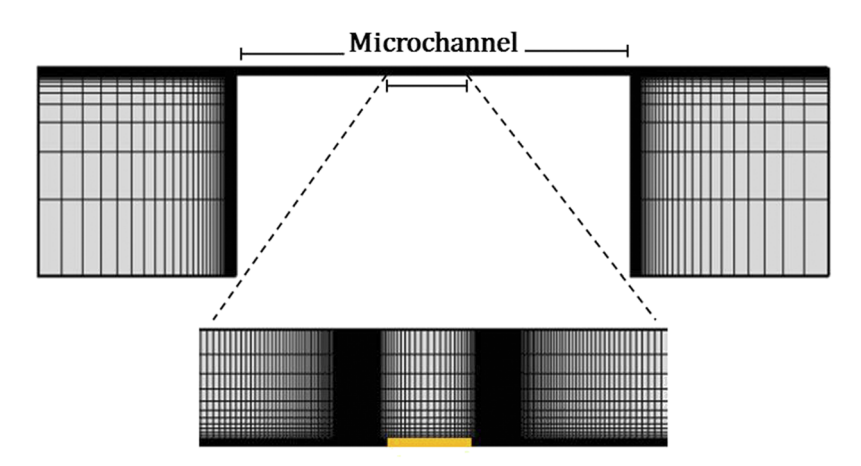


FIG. 4. Grid distribution in the microchannel with the zoomed area around the nanoporous membrane.

Nanoporous membrane

The equations for the enrichment factor and ionic conductivity (*G*) using quadratic model in terms of parameters (30 < A < 90, 5 < B < 30, 0.01 < C < 10) could be expressed in the following form:

$$EF = 73\,288.06 - 144.83A - 1636.86B - 12\,512.35C + 12.21AB$$

$$-0.65AC - 0.65AC - 99.3BC - 0.19A^2 + 21.22B^2 + 951.09C^2,$$
 (7)

$$G = 7.864 \times 10^{-9} + 1.662 \times 10^{-9} A + 1.695 \times 10^{-8} B + 2.531 \times 10^{-8} C$$
$$+ 4.438 \times 10^{-8} AB - 7.355 \times 10^{-8} AC + 1.05 \times 10^{-8} BC$$
$$- 1.422 \times 10^{-9} A^2 + 5.949 \times 10^{-9} B^2 - 1.38 \times 10^{-8} C^2, \tag{8}$$

A. Analysis of variance (ANOVA)

The qualities of the fitted results obtained from the RSM [Eqs. (7) and (8)] were analyzed through ANOVA for finding inter-relations among the governing parameters. We used sum of squares, degree of freedom (DOF), mean squares, F-value, and p-value (Tables IV and V). The statistical significance of the numerical data was determined by the F-value, which had more precision for F-values higher than one. F-values of 69.18 and 8.59 for the enrichment factor and ionic conductivity implied that our models were meaningful. P-values less than 0.05 indicated that the model terms were significant. For instance, the buffer concentration (C), squares of the buffer concentration (C^2), and the interaction between length and voltage (AB) were significant terms for the enrichment factor.

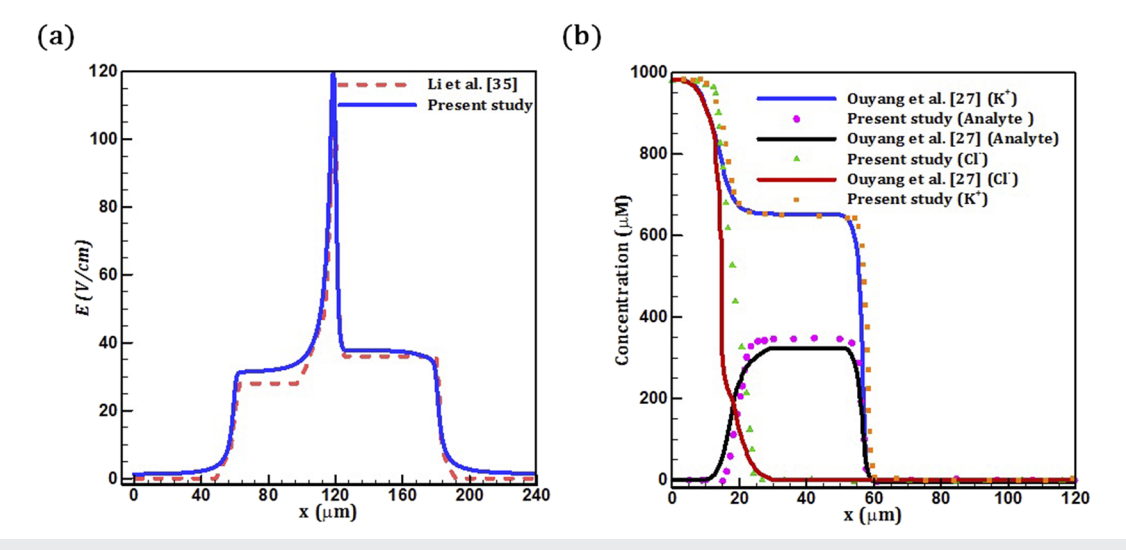


FIG. 5. Comparison between the present study and the studies of Li et al.³⁵ and Ouyang et al.²⁷: (a) electric field distribution ($V_{cm} = 4V_T$)³⁵ and (b) concentration distribution of KCI solution and analyte in $V_{cm} = 30V_T$ at the microchannel centerline.²⁷

TABLE II. Levels of input parameters.

		Parameter ranges			
Parameters (non-dimensional)	Symbol	Low (−1)	Mean (0)	High (+1)	
Microchannel length	A: L _m ∕h	30	60	90	
Voltage difference	B: $\Delta V/V_T$	5	17.5	30	
Buffer concentration	C: C_{buffer}/C_0	0.01	5.005	10	

 R^2 and R^2_{adj} values for both cases were close to 1, indicating the correspondence of the predicted values to the actual values of the simulations. Adeq Precision compared the range of predicted values to average prediction error, and the desirable ratio was achieved for values greater than 4. Adeq Precision of 28.606 and 11.079 implied that our models could be used for design purpose.

VI. RESULTS

Figures 6(a) and 6(b) show variations of the enrichment factor with respect to the buffer concentration and dimensionless length of the microchannel for high ($\Delta V/V_T = 30$) and low ($\Delta V/V_T = 5$) voltages, respectively. The highest enrichment factor was observed for the low buffer concentration in both cases, while the increase in the buffer concentration led to the reduction in the enrichment factor.²⁹ For a specific microchannel length, the trend of enrichment factor values changed around $C_{buffer}/C_0 \cong 7$. Upon a further increase

in the buffer concentration (after $C_{buffer}/C_0 \cong 7$), the enrichment factor was preserved. This can be attributed to the limited counterions (H⁺) passing through the nanoporous membrane. The quantity of counterions, determined by net surface charges of the nanoporous membrane, was assumed to be constant in the nanoporous membrane ($C_{\text{H}^+} = 2$ mM). Thus, an increase in the buffer concentration allowed more DNA molecules to be replaced with buffer anions (Cl⁻). Such replacements lead to higher enrichment factors.

An enrichment factor value of around 1 was observed for high buffer concentrations at high voltages for a short microchannel or at low voltage for a long microchannel. This means that the accumulation of DNA molecules could not be accomplished for these design ranges. The reason for this was the balance of forces on DNA molecules. If low voltages were applied along a long microchannel, weak electroosmotic and electrophoretic forces were not sufficient to withstand the repulsion of DNA molecules at the nanoporous membrane. On the other hand, in a short microchannel with high

TABLE III. Proposed runs for the input parameters by the design of experiment software and the obtained results from simulations.

Run	L_m/h	$\Delta V/V_T$	C_{buffer}/C_0	EF	Max conductance (S)
1	60	17.50	5.00	8 817.12	9.67×10^{-9}
2	42.16	10.07	2.03	31 041.7	1.60×10^{-8}
3	77.84	21.00	2.03	34 396.33	1.80×10^{-8}
4	77.84	24.93	7.98	8 817.12	1.33×10^{-8}
5	60	17.50	5.00	8 817.12	9.67×10^{-9}
6	42.16	10.07	7.98	10 291.03	1.57×10^{-7}
7	60	5.00	5.00	8 747.27	1.10×10^{-8}
8	77.84	10.07	7.98	4 597.92	7.13×10^{-9}
9	77.84	10.07	2.03	29 049.73	1.65×10^{-8}
10	60	17.50	5.00	8 817.12	9.67×10^{-9}
11	42.16	21.93	7.98	10774.52	1.86×10^{-7}
12	90	17.50	5.00	6 123.43	6.64×10^{-9}
13	42.16	24.93	2.03	31 059.86	1.60×10^{-8}
14	60	17.50	5.00	8 817.12	9.67×10^{-9}
15	30	17.50	5.00	7 036.48	1.05×10^{-9}
16	60	30.00	5.00	10 291.03	1.35×10^{-8}
17	60	17.50	5.00	8 817.12	9.67×10^{-9}
18	60	17.50	0.01	50 320.25	3.47×10^{-9}
19	60	17.50	5.00	8 817.12	9.67×10^{-9}
20	60	17.50	10.00	5 073.98	1.14×10^{-8}

TABLE IV. ANOVA results for the enrichment factor.

Source	Sum of squares	DOF	Mean squares	F-value	p-value
Model	2.99×10^{9}	9	3.32×10^{8}	69.18	<0.0001
A	4 305 058	1	4 305 058	0.78	0.3994
В	2 604 081	1	2 604 081	0.47	0.5088
C	2.03×10^{9}	1	2.03×10^{9}	369.16	< 0.0001
AB	48 834 513	1	48 834 513	88.88	< 0.0001
AC	27 793.8	1	27 793.8	0.0005	0.9449
BC	22 356 726	1	22 356 726	4.06	0.0746
A^2	906 025.6	1	906 025.6	0.16	0.6943
B^2	12 271 345	1	12 271 345	2.23	0.1695
C^2	8.64×10^{9}	1	8.64×10^{9}	156.99	< 0.0001
Residual	49 508 319	9	5 500 924		
Lack of fit	49 508 319	4	12 377 080		
Pure error	0	5	0		
Total	3.03×10^{9}	18			
$R^2 = 0.9837$	$R_{adj}^2 = 0.9674$	Adeq Precision = 28.606	A: L_m/h	B: $\Delta V/V_T$	C: C_{buffer}/C_0

voltage, strong electroosmotic flow and electrophoretic forces were dominated. In such cases, the forces on DNA molecules were unbalanced and practically no accumulation of particles could be accomplished.

Figures 7(a) and 7(b) show the effects of voltage and nondimensional microchannel length on the enrichment factor for dimensionless buffer concentrations of 1 and 10. The highest enrichment factor occurred in a case where both voltage and length of the microchannel had higher values ($L_m/h > 60$ and $\Delta V/V_T > 20$). However, in experimental studies, excessive voltage could not be applied to the system due to the effect of the Joule heating as well as the change in molecule characteristic properties.³⁷ To overcome this limit, by changing the length and voltage, similar values for the enrichment factor could be obtained at a fixed buffer concentration. For example, at $C_{buffer}/C_0=1$, for $L_m/h\cong 55$ and $\Delta V/V_T=5$, the enrichment factor was similar to the case with $L_m/h=90$ and $\Delta V/V_T\cong 15$. In this way, for a specific enrichment factor, few sets of working conditions (voltage and channel length) could be considered for the device design.

Figures 8(a) and 8(b) show the effects of voltage and concentration on the enrichment factor for $L_m/h = 30$ and 90, respectively. The increase in the buffer concentration results in the decrease in the enrichment factor. However, with voltage enhancement, the enrichment factor did not increase. It could be concluded that among these two parameters, the effect of the buffer concentration was dominant. A comparison of Fig. 8(a) with Fig. 8(b) reveals that shorter

TABLE V. ANOVA for the ion conductivity.

Source	Sum of squares	DOF	Mean squares	F-value	p-value
Model	1.25×10^{-14}	9	1.39×10^{-15}	8.59	< 0.0001
A	1.56×10^{-17}	1	1.56×10^{-17}	0.10	0.8239
В	2.22×10^{-15}	1	2.22×10^{-15}	15.30	< 0.0001
C	1.5×10^{-15}	1	1.5×10^{-15}	10.36	0.0831
AB	2.84×10^{-15}	1	2.84×10^{-15}	19.61	< 0.0001
AC	9.11×10^{-16}	1	9.11×10^{-16}	6.29	0.1265
BC	1.85×10^{-15}	1	1.85×10^{-15}	12.81	< 0.0001
A^2	2.44×10^{-17}	1	2.44×10^{-17}	0.16	0.7815
B^2	2.65×10^{-16}	1	2.65×10^{-16}	1.82	0.376
C^2	6.42×10^{-16}	1	6.42×10^{-16}	4.43	0.1869
Residual	1.74×10^{-15}	6	2.89×10^{-16}		
Lack of fit	1.74×10^{-15}	1	1.74×10^{-15}		
Pure error	0	5	0		
Total	1.42×10^{-14}	15			
$R^2 = 0.8780$	$R_{adj}^2 = 0.7051$	Adeq Precision = 11.079	A: L_m/h	B: $\Delta V/V_T$	C: C_{buffer}/C_0

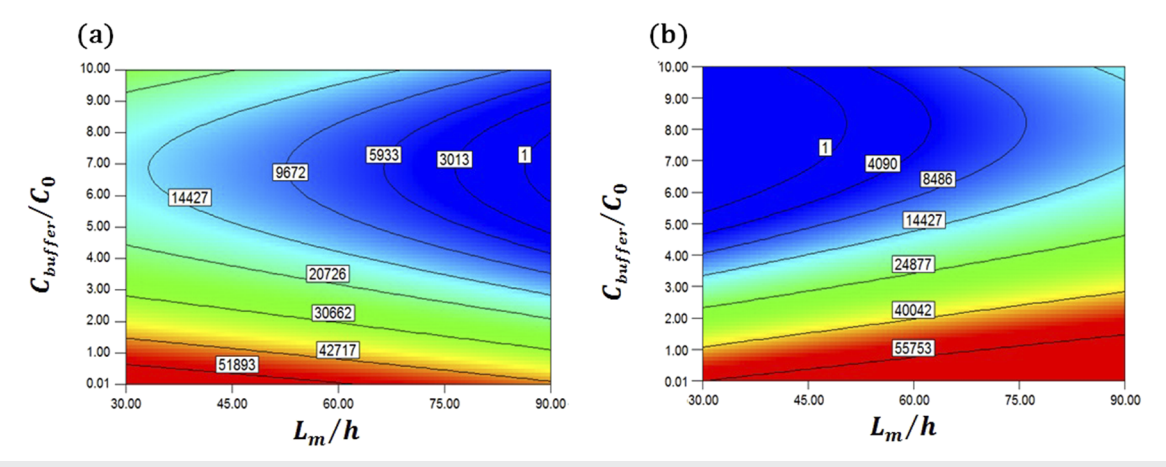


FIG. 6. Variations of the enrichment factor based on the concentration and dimensionless length of the microchannel for (a) $\Delta V/V_T = 5$ and (b) $\Delta V/V_T = 30$.

lengths ($L_m/h = 30$) have a larger region with the enrichment factor of 1 [dark blue part in top right of Fig. 8(a)], meaning that channels with short length are more susceptible to fail preconcentrating an analyte.

An electric field value proposed by ANOVA is given to Table VI for a fixed buffer concentration ($C_{buffer}/C_0 = 1$). The proposed length and voltage through optimization were suggested in a way that the applied electric field remained in a confined range (20 V/cm-30 V/cm). This finding is in a good agreement with the reported experimental studies. For example, Kim *et al.*³⁷ demonstrated an applicable device to preconcentrate 10^{-4} mM FITC-labeled BSA protein in 1 mM PBS buffer, which had the exact values of molecules and buffer concentration in our simulation. They used 25 V/cm as optimal electric field to avoid Joule heating and maximize the enrichment factor. Our finding is in agreement with their reported electric field. In another research, Chang and Yang, ³⁸ who used graphene oxide–Nafion (GO–Nafion) to increase the enrichment

factor, observed the maximum amount of enrichment factor for fluorescein using an electric field of 20 V/cm. In addition, Kim *et al.* 30 employed an electric field of 33.33 V/cm for preconcentration of red blood cell (RBC) out of diluted human whole blood using buffer concentrations from 0.1 mM to 36.5 mM.

In the following section, the effects of the parameters on ionic conductivity are studied. Figures 9(a) and 9(b) show the ionic conductivity contour based on the non-dimensional concentration and microchannel length for low and high voltages, respectively. For short microchannel length, the ionic conductivity was enhanced with buffer concentration. In this case, a shorter microchannel leads to a lower space charge density and the ionic conductivity is dominated by the buffer concentration behavior. On the other hand, the buffer concentration had less effect on the ionic conductivity for higher microchannel length (higher surface charge) and no significant enhancement in conductivity was observed. It could be concluded that for small microchannel length, ionic conductivity was

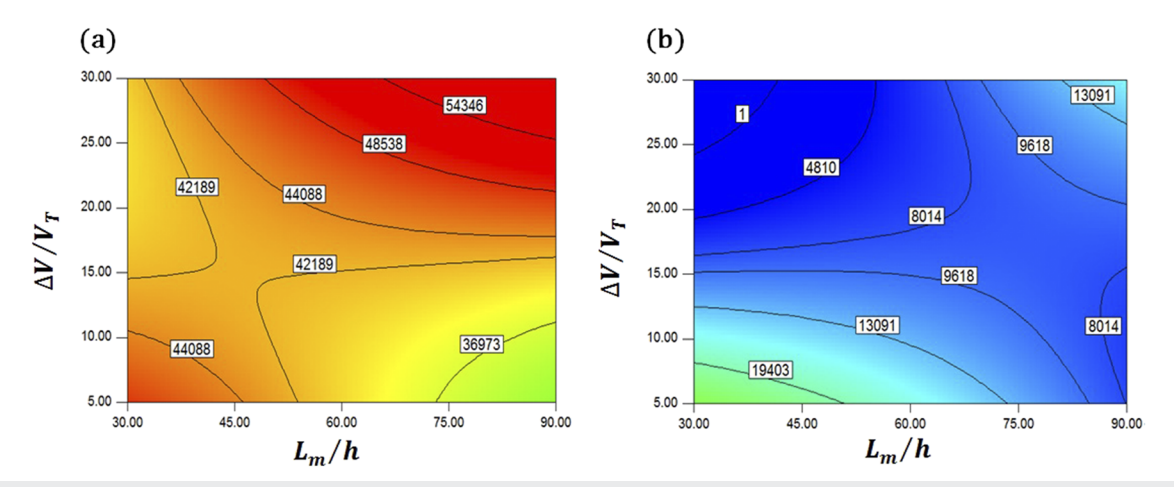


FIG. 7. Variations of the enrichment factor based on the dimensionless voltage and length of the microchannel: (a) $C_{buffer}/C_0 = 1$ and (b) $C_{buffer}/C_0 = 10$.

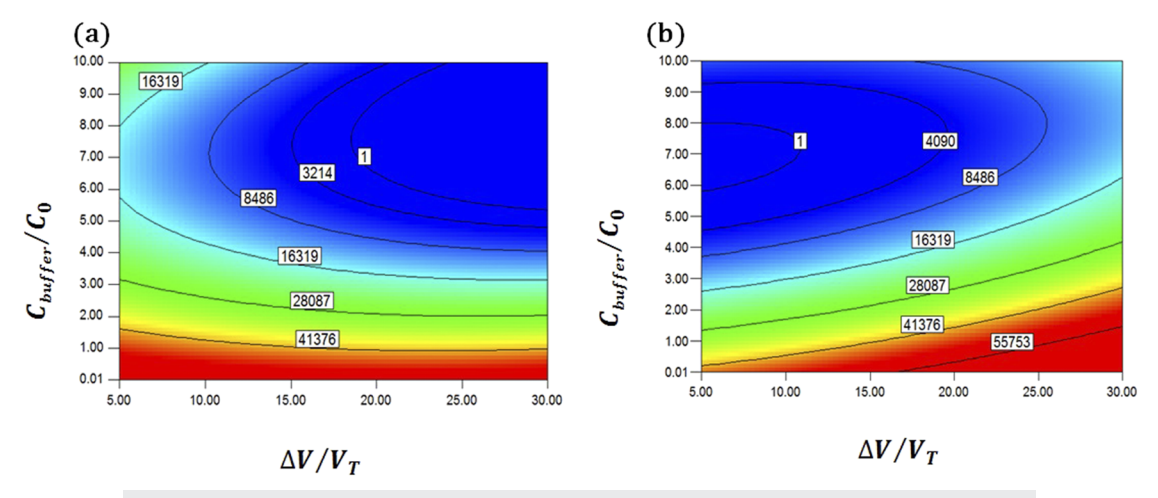


FIG. 8. Variations of the enrichment factor based on the concentration and voltage: (a) $L_m/h = 30$ and (b) $L_m/h = 90$.

almost independent of low buffer concentration ($C_{buffer}/C_0 \ll 1$), which was in agreement with previously reported studies.^{39,40}

The effects of concentration and voltage on conductivity for short and long microchannel lengths are shown in Figs. 10(a) and 10(b). With the increment of applied voltage for long microchannel length ($L_m/h = 90$), the ionic conductivity increased. This trend was in agreement with the results of Yeh *et al.*³² They found that at a low ionic concentration ($C_{buffer} < 1$ mM), an increase in voltage could enhance the ionic conductivity in ICP-based devices. The reason behind this feature relies on the fact that for higher voltages that induce stronger electroosmotic flow, space charge density (ρ_E) was more effective on the ionic conductivity compared to the effect of the buffer concentration on ionic conductivity.³⁵ On the other hand, for short microchannel lengths, voltage plays a more effective role than buffer concentration, and the highest conductivity was achieved at low voltages.

By examining the interactions of voltage and microchannel length in Figs. 11(a) and 11(b), it could be concluded that the highest ionic conductivity was achieved for high voltage in a long microchannel (or vice versa). It was observed that by choosing an appropriate microchannel geometry and proper voltage, the conductivity could be significantly enhanced.

The optimized model (E = 24 V/cm) was employed to predict the conductivity of a device comprised of a nanojunction in a microchannel, and the predictions were compared with the literature $^{39,41-43}$ (Fig. 12). The findings revealed that conductivity did not change at low buffer concentrations. In this range, the channel geometry, i.e., the length, height, or surface charge of a channel, and the applied voltage were dominant parameters on ionic conductivity. On the other hand, the conductivity in high buffer concentrations ($C_{buffer} \geq 1$ mM) was mainly governed by the buffer concentration. For a given channel, the conductivity increased with the buffer

TABLE VI. Suggested length and voltage at a certain buffer concentration to achieve the maximum enrichment factor, EF_{max}

Run	L_m/h	$\Delta V/V_T$	C_{buffer}/C_0	$\mathrm{EF}_{\mathrm{max}}$	Electric field (V/cm)
Number	Suggested	Suggested	Defined	Predicted	Calculated
1	81.605	26.65	1.00	54 642.08	21.06
2	71.21	25.49	1.00	50 864.18	23.09
3	81.625	21.19	1.00	47 685.13	18.74
4	73.98	21.18	1.00	46 887.00	18.47
5	31.78	11.62	1.00	43 394.33	23.58
6	59.97	26.80	1.00	49 409.42	28.82
7	40.6	11.37	1.00	42 888.09	18.06
8	44.8	10.12	1.00	42 779.24	19.58
9	58.375	25.06	1.00	47 598.43	27.69
10	31.88	15.18	1.00	42 004.53	30.71
11	54.43	29.54	1.00	50 054.59	31.00
12	56.19	19.55	1.00	43 878.77	22.44

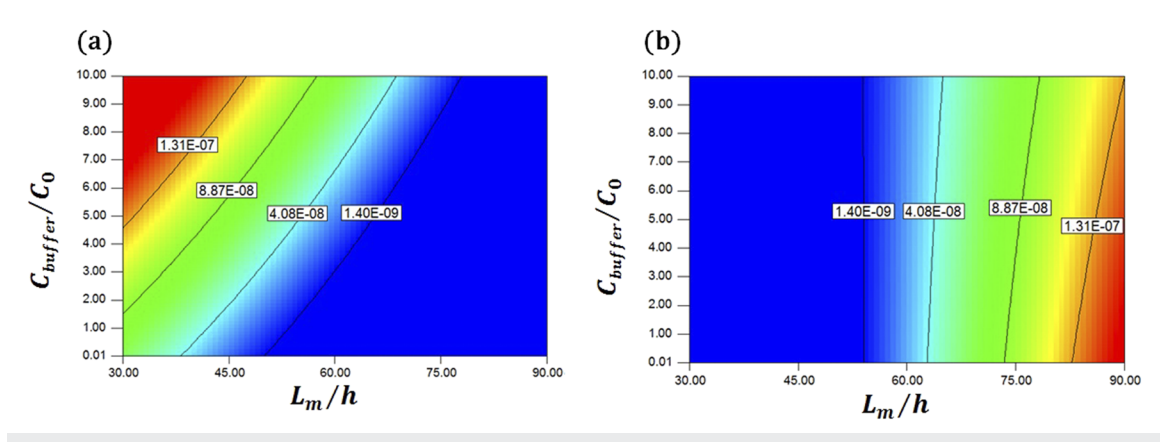


FIG. 9. Variations of conductivity based on the concentration and dimensionless length of the microchannel for (a) $\Delta V/V_T = 5$ and (b) $\Delta V/V_T = 30$.

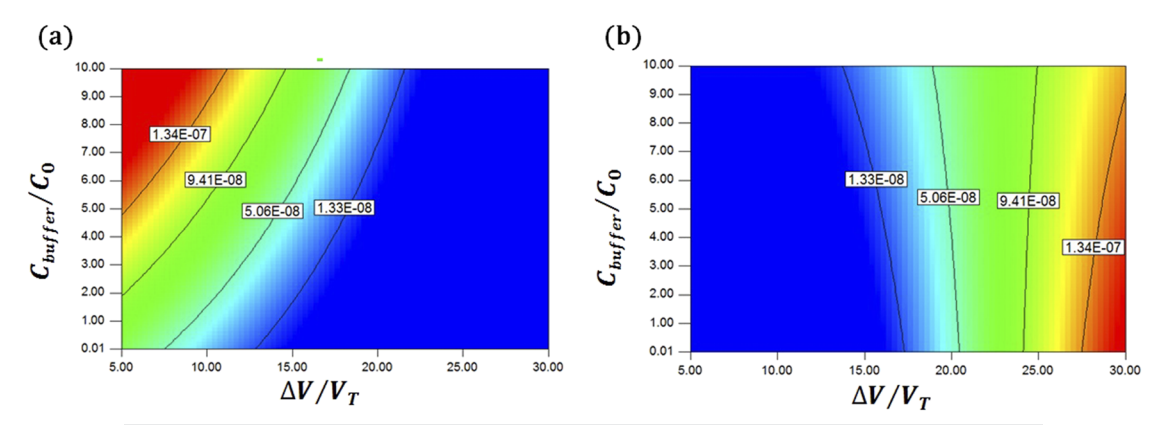


FIG. 10. Variations of conductivity based on the buffer concentration and voltage for (a) $L_m/h = 30$ and (b) $L_m/h = 90$.

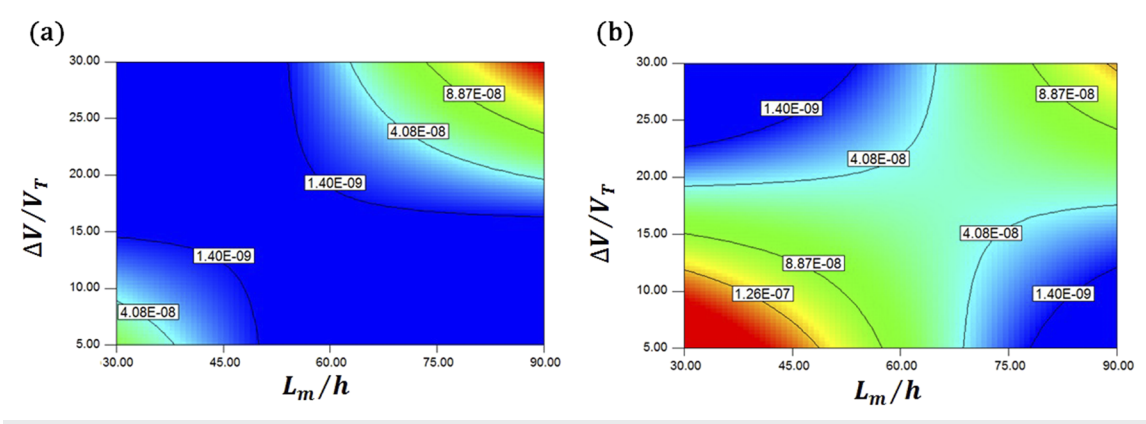


FIG. 11. Variations of conductivity based on the dimensionless voltage and length of the microchannel for (a) $C_{buffer}/C_0 = 1$ and (b) $C_{buffer}/C_0 = 10$.

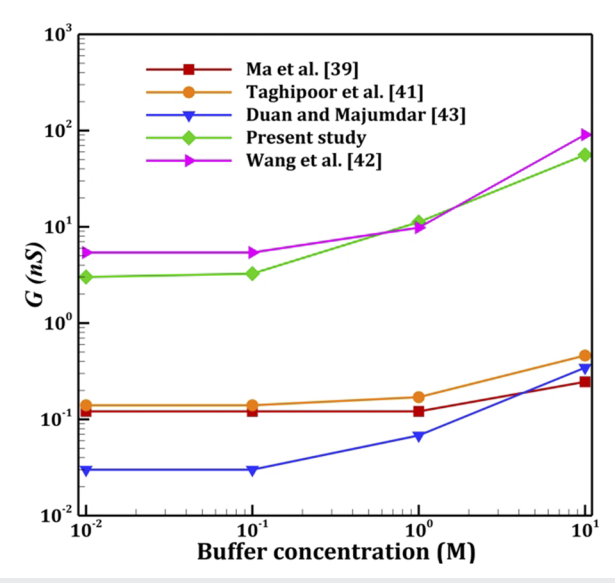


FIG. 12. Comparison of the result of the present study at an electric field of 24 V/cm with the results of Ma *et al.*, ³⁹ Taghipoor *et al.*, ⁴¹ Wang *et al.*, ⁴² and Duan and Majumdar. ⁴³

concentrations due to an increase in convection for both negative and positive ions in buffer solution and diminishes the influence of channel characteristics. In this case, the conductivity enhanced linearly as the buffer concentration increased.

VII. CONCLUSION

Preconcentration of charged molecules using ICP devices requires interplay between electroosmotic forces, electrophoretic forces, and repulsion forces at the vicinity of nanochannels. These forces could be affected by various parameters including buffer concentration, applied voltage, and device geometry. The RSM analysis revealed the effects of the governing parameters and their interactions on the enrichment factor and ionic conductivity. It is a practical approach to analyze the importance of the interactions between the applied voltage and the microchannel length for the enrichment factor and ionic conductivity in ICP-based devices. The effect of the buffer concentration on the enrichment factor was dominant compared to the other parameters. In addition, the ionic conductivity was not affected considerably by the increment of the buffer concentration up to 0.1 mM (C_{buffer} < 0.1 mM). On the other hand, the device geometry (length and height of a microchannel) and the applied voltage could significantly influence ionic conductivity, which was also shown through experimental and analytical studies. 40,44 Some experimental studies have reported that an inappropriate geometry design and voltage difference could decrease the enrichment factor and preconcentration molecule accumulation.²³ To achieve a proper enrichment factor, based on RSM optimization, an electric field of 20 V/cm-30 V/cm was suggested as an initial operating value to improve preconcentration efficiency of charged molecules for a certain buffer concentration (~1 mM) in ICP-based devices.

SUPPLEMENTARY MATERIAL

See Fig. S1 in the supplementary material for a comparison of the contour of DNA concentration distribution in our model compared to experimental and numerical studies of Ouyang *et al.*²⁷

ACKNOWLEDGMENTS

S.A.M.S. gratefully acknowledges funding by the National Institute for Medical Research Development (NIMAD) under Grant No. 957144.

DATA AVAILABILITY

The data that support the findings of this study are available from the corresponding author upon reasonable request.

REFERENCES

- ¹ A. Razmjou *et al.*, "Design principles of ion selective nanostructured membranes for the extraction of lithium ions," Nat. Commun. **10**(1), 5793 (2019).
- ²M. Li and R. K. Anand, "Recent advancements in ion concentration polarization," Analyst 141(12), 3496–3510 (2016).
- ³ A. J. Moghadam, "Unsteady electrokinetic flow in a microcapillary: Effects of periodic excitation and geometry," J. Fluids Eng. 141, 111104 (2019).
- ⁴B. Ma, J. Chi, and H. Liu, "Fabric based ion concentration polarization for pump-
- free water desalination," ACS Sustainable Chem. Eng. **6**, 99–103 (2017).

 S. J. Kim *et al.*, "Direct seawater desalination by ion concentration polarization,"
- Nat. Nanotechnol. 5, 297 (2010).

 ⁶D. Kim *et al.*, "Non-equilibrium electrokinetic micro/nano fluidic mixer," Lab
- Chip 8(4), 625–628 (2008).

 O Jännig and N.-T. Nguyen, "A polymeric high-throughput pressure-driven
- micromixer using a nanoporous membrane," Microfluid. Nanofluid. **10**(3), 513–519 (2011).
- ⁸W. Liu *et al.*, "A universal design of field-effect-tunable microfluidic ion diode based on a gating cation-exchange nanoporous membrane," Phys. Fluids **29**(11), 112001 (2017).
- ⁹H. Lee *et al.*, "A concentration-independent micro/nanofluidic active diode using an asymmetric ion concentration polarization layer," Nanoscale **9**(33), 11871–11880 (2017).
- ¹⁰C.-C. Chao, P.-H. Chiu, and R.-J. Yang, "Preconcentration of diluted biochemical samples using microchannel with integrated nanoscale Nafion membrane," Biomed. Microdevices 17(2), 25 (2015).
- ¹¹H. Cui et al., "Isoelectric focusing in a poly(dimethylsiloxane) microfluidic chip," Anal. Chem. 77(5), 1303–1309 (2005).
- ¹²M. Hügle *et al.*, "A lab-on-a-chip for free-flow electrophoretic preconcentration of viruses and gel electrophoretic DNA extraction," Analyst 145(7), 2554–2561 (2020)
- ¹³R. D. Oleschuk *et al.*, "Trapping of bead-based reagents within microfluidic systems: On-chip solid-phase extraction and electrochromatography," Anal. Chem. **72**(3), 585–590 (2000).
- ¹⁴S.-J. Liang et al., "Research and application progress of paper-based microfluidic sample preconcentration," Chin. J. Anal. Chem. 47(12), 1878–1886 (2019).
- ¹⁵C. Zhao, Z. Ge, and C. Yang, "Microfluidic techniques for analytes concentration," Micromachines 8(1), 28 (2017).
- ¹⁶S. A. Hong *et al.*, "Electrochemical detection of methylated DNA on a microfluidic chip with nanoelectrokinetic pre-concentration," Biosens. Bioelectron. 107, 103–110 (2018).
- ¹⁷J.-C. Niu *et al.*, "Simultaneous pre-concentration and separation on simple paper-based analytical device for protein analysis," Anal. Bioanal. Chem. **410**(6), 1689–1695 (2018).

- ¹⁸A. Perera *et al.*, "Rapid pre-concentration of *Escherichia coli* in a microfluidic paper-based device using ion concentration polarization," *Electrophoresis* **41**, 867–874 (2019).
- ¹⁹C.-P. Jen *et al.*, "Protein preconcentration using nanofractures generated by nanoparticle-assisted electric breakdown at junction gaps," PLoS One **9**(7), e102050 (2014).
- ²⁰Y.-C. Wang, A. L. Stevens, and J. Han, "Million-fold preconcentration of proteins and peptides by nanofluidic filter," Anal. Chem. 77(14), 4293–4299 (2005).
- ²¹M. M. Gong *et al.*, "Direct DNA analysis with paper-based ion concentration polarization," J. Am. Chem. Soc. **137**(43), 13913–13919 (2015).
- ²²H. Gao *et al.*, "Electrokinetic stacking on paper-based analytical device by ion concentration polarization with ion exchange membrane interface," Microfluid. Nanofluid. 22(5), 50 (2018).
- ²³ X. Yuan *et al.*, "Electrokinetic biomolecule preconcentration using xurography-based micro-nano-micro fluidic devices," Anal. Chem. **87**(17), 8695–8701 (2015).
 ²⁴ L. Gong, Z. Li, and J. Han, "Numerical simulation of continuous extraction of highly concentrated Li⁺ from high Mg²⁺/Li⁺ ratio brines in an ion concentration polarization-based microfluidic system," Sep. Purif. Technol. **217**, 174–182 (2019).
- ²⁵L. Gong *et al.*, "Direct numerical simulation of continuous lithium extraction from high Mg²⁺/Li⁺ ratio brines using microfluidic channels with ion concentration polarization," J. Membr. Sci. **556**, 34–41 (2018).
- ²⁶ J. Wang, L.-l. Han, and Z. Xu, "Nano-electrokinetic ion concentration in the ion enrichment zone," Microsyst. Technol. 25, 711–717 (2018).
- ²⁷W. Ouyang *et al.*, "Deciphering ion concentration polarization-based electrokinetic molecular concentration at the micro-nanofluidic interface: Theoretical limits and scaling laws," Nanoscale **10**, 15187–15194 (2018).
- ²⁸ M. Jia and T. Kim, "Multiphysics simulation of ion concentration polarization induced by nanoporous membranes in dual channel devices," Anal. Chem. **86**(15), 7360–7367 (2014).
- ²⁹ M. Jia and T. Kim, "Multiphysics simulation of ion concentration polarization induced by a surface-patterned nanoporous membrane in single channel devices," Anal. Chem. **86**(20), 10365–10372 (2014).
- ³⁰J. Kim *et al.*, "Ion concentration polarization by bifurcated current path," Sci. Rep. 7(1), 5091 (2017).

- ³¹ J. Kamcev *et al.*, "Salt concentration dependence of ionic conductivity in ion exchange membranes," J. Membr. Sci. **547**, 123–133 (2018).
- ³²L.-H. Yeh et al., "Ion concentration polarization in polyelectrolyte-modified nanopores," J. Phys. Chem. C 116(15), 8672–8677 (2012).
- ³³L. Gong et al., "Force fields of charged particles in micro-nanofluidic preconcentration systems," AIP Adv. 7(12), 125020 (2017).
- ³⁴C. L. Druzgalski, M. B. Andersen, and A. Mani, "Direct numerical simulation of electroconvective instability and hydrodynamic chaos near an ion-selective surface," Phys. Fluids 25(11), 110804 (2013).
- ³⁵Z. Li *et al.*, "Accurate multi-physics numerical analysis of particle preconcentration based on ion concentration polarization," Int. J. Appl. Mech. **9**(08), 1750107 (2017).
- ³⁶Y. Daghighi and D. Li, "Numerical studies of electrokinetic control of DNA concentration in a closed-end microchannel," Electrophoresis **31**(5), 868–878 (2010).
- ³⁷M. Kim, M. Jia, and T. Kim, "Ion concentration polarization in a single and open microchannel induced by a surface-patterned perm-selective film," Analyst 138(5), 1370–1378 (2013).
- ³⁸C.-H. Chang and R.-J. Yang, "Enhanced sample preconcentration in microfluidic chip using graphene oxide–Nafion membrane," Microfluid. Nanofluid. **20**(12), 168 (2016).
- ³⁹Y. Ma *et al.*, "pH-regulated ionic conductance in a nanochannel with overlapped electric double layers," Anal. Chem. **87**(8), 4508–4514 (2015).
- ⁴⁰D. Stein, M. Kruithof, and C. Dekker, "Surface-charge-governed ion transport in nanofluidic channels," Phys. Rev. Lett. **93**(3), 035901 (2004).
- ⁴¹M. Taghipoor, A. Bertsch, and P. Renaud, "An improved model for predicting electrical conductance in nanochannels," Phys. Chem. Chem. Phys. 17(6), 4160–4167 (2015).
- ⁴²M. Wang, Q. Kang, and E. Ben-Naim, "Modeling of electrokinetic transport in silica nanofluidic channels," Anal. Chim. Acta **664**(2), 158–164 (2010).
- ⁴³C. Duan and A. Majumdar, "Anomalous ion transport in 2-nm hydrophilic nanochannels," Nat. Nanotechnol. 5(12), 848 (2010).
- ⁴⁴Y. Green, S. Shloush, and G. Yossifon, "Effect of geometry on concentration polarization in realistic heterogeneous permselective systems," Phys. Rev. E **89**(4), 043015 (2014).